tions with moderate numbers of integration points the area has been divided into three different sections of identical size. The effective indices of the lowest order eigenmodes within the three

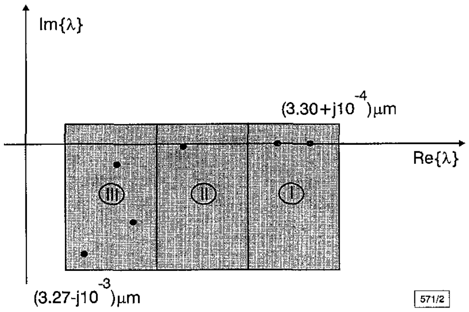


**Fig. 2** *Rectangular areas with determined eigenmodes*
● zeros within area

different areas are shown in Table 1. The accuracy of the computed propagation constants of the modes depends on the number of integration points. For the integration named '4 × 8' an eight point quadrature formula has been used at each side of the rectangle. The calculations '8 × 8' used the same integration formula but all sides of the rectangle were cut in halves. So, eight integrals have been computed by an 8 point formula. The results have been compared with the SVD algorithm [2]. Here, the start point has to be close to the unknown zero. Therefore, the calculation of all effective indices within the observed area can be time consuming.

**Table 1:** Computed effective indices for TE and TM modes

| Region | Mode | Integration | Cauchy | SVD |
|---|---|---|---|---|
| | | | µm | µm |
| I | 1st TE | 4 × 8 | $3.295816-j1.3494\times10^{-6}$ | $3.295816-j5.2059\times10^{-7}$ |
| | | 8 × 8 | $3.295816-j5.2168\times10^{-7}$ | |
| | 2nd TE | 4 × 8 | $3.293759-j5.2101\times10^{-6}$ | $3.293765-j6.6987\times10^{-7}$ |
| | | 8 × 8 | $3.293765-j6.6847\times10^{-7}$ | |
| II | 1st TM | 4 × 8 | $3.284214-j1.6983\times10^{-5}$ | $3.284211-j1.8198\times10^{-5}$ |
| | | 8 × 8 | $3.284210-j1.8209\times10^{-5}$ | |
| III | 2nd TM | 4 × 8 | $3.278504-j7.0639\times10^{-4}$ | $3.278508-j7.0932\times10^{-4}$ |
| | | 8 × 8 | $3.278508-j7.0937\times10^{-4}$ | |
| | 3rd TE | 4 × 8 | $3.276128-j1.4646\times10^{-4}$ | $3.276123-j1.4265\times10^{-4}$ |
| | | 8 × 8 | $3.276123-j1.4261\times10^{-4}$ | |
| | 4th TE | 4 × 8 | $3.272242-j9.4949\times10^{-4}$ | $3.272246-j9.5078\times10^{-4}$ |
| | | 8 × 8 | $3.272247-j9.5159\times10^{-4}$ | |

It can be seen that the integration '4 × 8' does not lead to accurate imaginary parts of the effective indices. For double the number of boundary elements, the results are closer to the values calculated by the SVD algorithm. The accuracy can be increased with Gaussian integration formulas of higher order or smaller observed areas. Using the algorithm proposed in this Letter, two TM and four TE eigenmodes have been determined in the whole area. Therefore, the algorithm is very suitable for the determination of several complex effective indices in only one computation step.

*Conclusion:* A method has been presented for the calculation of eigenmodes with complex effective indices. Cauchy's theorem was used in connection with the Gaussian integration formula. Effective indices were compared with values computed by an SVD algorithm. The proposed method can be used as an automatic computation algorithm for the determination of several zeros of a complex analytic function within a closed area.



27 July 1998
*Electronics Letters Online No: 19981256*

O. Conradi (*Allgemeine und Theoretische Elektrotechnik, Fern Universität Hagen, D-58084 Hagen, Germany*)

**References**


1 LABAY, V.A., and BORNEMANN, J.: 'Matrix singular value decomposition for pole-free solutions of homogeneous matrix equations as applied to numerical modeling methods', *Microw. Guid. Wave Lett.*,**2**, (2), pp. 49–51

2 KREMER, D.: 'Method of lines for the analysis of optical waveguide structures with complex refractive indices using a pole-free eigenvalue determination', *Electron. Lett.*, 1984, **30**, (13), pp. 1088–1090

3 REMMERT, R.: 'Theory of complex functions' (Springer Verlag, Berlin; Heidelberg; New York, 1991)

4 ABRAMOWITZ, M., and STEGUN, A.: 'Handbook of mathematical functions' (Dover Publications, New York, 1970), pp. 916–919

5 WILKINSIN, J.H.: 'The algebraic eigenvalue problem' (Clarendon Press, Oxford, 1965)

6 KREMER, D., and PREGLA, R.: 'MOLCAR a very efficient and accurate design tool for the hybrid analysis of multilayered waveguide structures'. SPIE, 1997, Vol. 2997, pp. 255–262


## Experimental demonstration of efficient all-optical code-division multiplexing

Jian-Guo Zhang, Lian-Kuan Chen and Wing C. Kwong

New experiments on all-optical code-division multiplexing (AO-CDM) are described. Unlike conventional designs, the proposed transmitter does not require an optical intensity modulator to on-off modulate ultrashort optical clock pulses. Moreover, the use of a $2^n$ prime code results in a simple AO-CDM encoder and decoder with an all-serial architecture. Thus, new systems based on the above will be more cost- and power-effective than conventional AO-CDM systems. The reduction in timing jitter is also considered.

*Introduction:* Optical code-division multiplexing (CDM) systems have been demonstrated [1 – 3]. Although the use of an optical address code with cross-correlation constraint $\lambda_c = 1$ can lead to a lower bit error rate than for $\lambda_c > 1$ [1], the system complexity and power loss must be also considered for all-optical CDM (AO-CDM). Recently, a study has shown that $2^n$ codes can be used to reduce the complexity of an AO-CDM encoder/decoder [2]. This is achieved by employing an all-serial architecture as shown in Fig. 1, resulting in fewer optical components and lower optical power loss than for a conventional all-parallel encoder/decoder. A silica-based planar lightwave circuit (PLC) can feasibly be used to implement this power-efficient, waveguide-integrable all-serial structure. Moreover, by integrating the silica-based PLC with an Er-doped silica waveguide amplifier [6], a lossless AO-CDM encoder (or decoder) can be also realised. In this Letter, we report new experiments on AO-CDM systems using $2^n$ prime code and

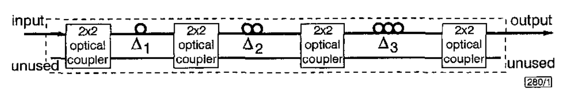


**Fig. 1** *All-serial encoder or decoder for* $2^n$ *prime code of* $n = 3$

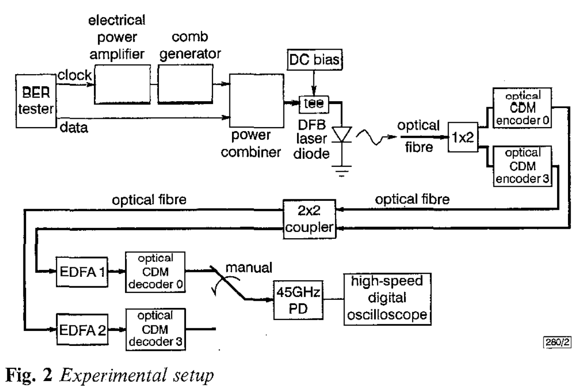


**Fig. 2** *Experimental setup*
EDFA: erbium-doped fibre amplifier, PD: photodetector

low-cost all-serial encoders/decoders. Unlike conventional AO-CDM systems [1 – 3], the proposed transmitter does not require an optical intensity modulator, and therefore, the new AO-CDM systems will be more cost- and power-effective than conventional systems.

*Principle and experiment:* The experimental setup is shown in Fig. 2. The codewords used in this experiment are the 0th and 3rd codewords of a $2^n$ prime code with $\lambda_c = 2$, code weight 8, code size 11, and length $L = 121$ for $n = 3$, as constructed in [4], i.e. $C_0 = (XX1E1E1E1E1E1E1EX)$ and $C_3 = (XX$ 00000010000 00000000010 01000000000 00001000000 00000001000 $E1$ 00100000000 000 00100000 $X)$, where $X$ and $E$ denote 11 and 10 adjacent zeros in a sub-sequence, respectively. Assume that the data rate $f_d$ is 100Mbit/s. The slot width $\tau$ is then equal to $1/f_dL$ = 82.6ps.

As shown in Fig. 2, the 100MHz electrical clock signal is used to drive a comb generator of which the output signal is added to the 100Mbit/s electrical data at the transmitting end. Then a 1.55μm distributed feedback (DFB) laser diode (LD) is driven by a current signal containing three components (i.e. a DC prebias, a data current pulse, and a clock pulse). By correctly setting the prebias and data currents, the DFB LD is biased just below the threshold at which gain switching occurs. The LD is gain switched only if a data pulse and a clock pulse are simultaneously present so that the carrier concentration above the threshold [5]. Thus, the ultrashort optical clock signal is modulated by electrical data bits at the LD, without using any optical intensity modulator. The resulting optical pulse is then fed into AO-CDM encoder $i$ to generate codeword $C_i$ ($i$ = 0 and 3). For a $2^n$ codeword of $n = 3$, the all-serial encoder (or decoder) comprises only $n + 1 = 4$ passive optical $2 \times 2$ couplers and six optical delay lines which are the pigtail fibres of low-cost $2 \times 2$ couplers (see Fig. 1); while an all-parallel encoder (or decoder) requires 14 optical $1 \times 2$ couplers and eight optical fibres [2]. Thus, use of the all-serial structure can reduce the complexity and power loss of AO-CDM encoders/decoders, especially for large $n$.

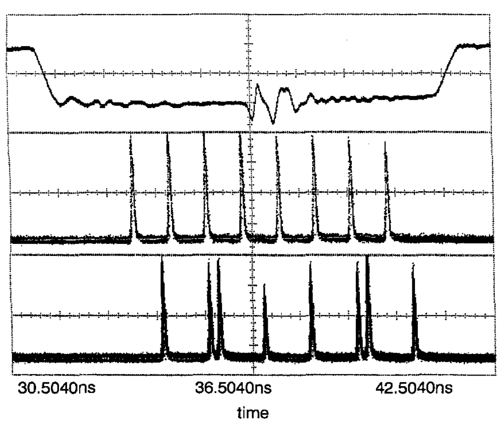


**Fig. 3** *Electrical data bit and optical pulse sequences encoded with $C_0$ and $C_3$*

Timebase: 1.20ns/div

An electrical NRZ data bit '1' (with ECL logic) is shown in Fig. 3 (upper trace). The corresponding codewords $C_0$ and $C_3$ from two optical encoders are shown as the middle and lower traces in Fig. 3. The optical clock pulse used has a pulsewidth of 64ps. Although commercially available low-cost $2 \times 2$ optical couplers are used in the encoders/decoders, nearly constant-amplitude optical pulses are obtained for $C_0$, by using couplers of 2.9dB/3.1dB splitting ratio as well as carefully cutting and fusing pigtail fibres between two couplers. In the experiment, we can control the time error of the fibre delay lines within 17ps as measured. For $C_3$, unequal pulse amplitudes are visible because optical $2 \times 2$ couplers with a worse ratio are used. This also suggests that the use of a silica-based PLC should lead to low power loss, uniform splitting ratio, and very precise time delay for all-serial encoders/decoders. With the silica-based PLC, a power-efficient, waveguide-integrable AO-CDM encoder or decoder can be feasibly implemented. The autocorrelation of $C_0$ is measured at the output of decoder 0, which has a main peak of 8 and highest sidelobe of 7 (see Fig. 4*a*), because $C_0$ is of a repetition code. The cross-correlation of $C_0$ with $C_3$ is shown in Fig. 4*b*. Although a gain-switched DFB LD suffers both timing jitter and frequency chirping, they can be reduced by injecting a CW light of narrow linewidth (from an external tunable source) into the gain-switched LD. Fig. 5 shows the measured gain-switching optical pulses without and with optical-injection locking in our experiment. The RMS timing jitter, measured from the *HP* high-speed digital oscilloscope, is reduced from 7.2 to 3.7ps by using this scheme with a injection power of 155μw at 1.55μm.

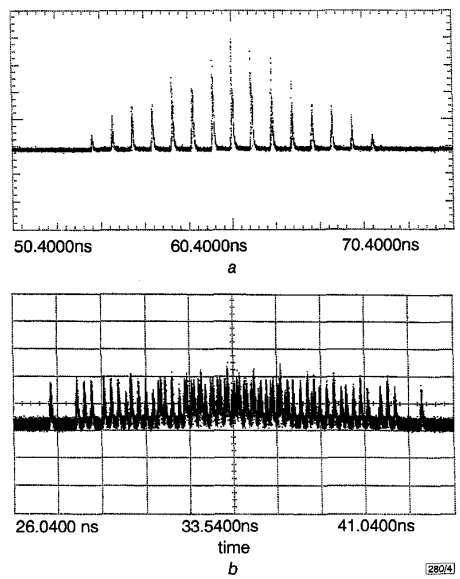


**Fig. 4** *Measured results*

*a* Autocorrelation of $C_0$
Timebase: 2.0ns/div, channel: 50mV/div
*b* Cross-correlation of $C_0$ with $C_3$
Timebase: 1.5ns/div, channel: 20mV/div

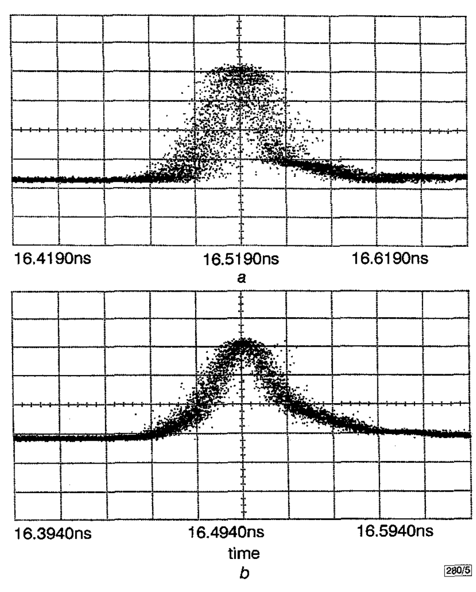


**Fig. 5** *Measured gain-switching optical clock pulses*

*a* Without optical-injection locking
*b* With optical-injection locking

In condusion, we have demonstrated high-speed AO-CDM using a $2^n$ prime code and low-cost all-serial encoders/decoders. Since no optical intensity modulators are required, cost- and power-effective AO-CDM systems can be realised. The encoders and decoders are waveguide-integrable.

 26 July 1998

Electronics Letters Online No: 19981274

Jian-Guo Zhang (*Telecommunications Program, School of Advanced Technologies, Asian Institute of Technology, PO Box 4, Klong Luang, Pathumthani 12120, Thailand*)

E-mail: jgzhang@cs.ait.ac.th

Lian-Kuan Chen (*Department of Information Engineering, The Chinese University of Hong Kong, Shatin, NT, Hong Kong*)

Wing C. Kwong (*Department of Engineering, Hofstra University, Hempstead, NY 11550, USA*)

## References

1 GAGLIARDI, R.M., MENDEZ, A.J., DALE, M.R., and PARK, E.: 'Fiber-optic digital video multiplexing using optical CDMA', *J. Lightwave Technol.*, 1993, **LT-11**, (1), pp. 20–26

2 KWONG, W.C., and PRUCNAL, P.R.: 'Ultrafast all-optical code-division multiple-access (CDMA) fiber-optic networks', *Computer Networks and ISDN Systems*, 1994, **26**, (6), pp. 1063–1086

3 PENDOCK, G.J., CAHILL, M.J.L., and SAMPSON, D.D.: 'Multi-gigabit per second demonstration of photonic code-division multiplexing', *Electron. Lett.*, 1995, **31**, (10), pp. 819–820

4 KWONG, W.C., and YANG, G.-C.: 'Construction of $2^n$ prime-sequence codes for optical code division multiple access', *IEE Proc. Commun.*, 1995, **142**, (3), pp. 141–150

5 LU, Y.-C., ZHOU, P., and CHENG, J.: 'A directly modulated pulse-compressed and time-multiplexed optical source for high-speed multiple-access networks', *IEEE Photonics Technol. Lett.*, 1993, **5**, (8), pp. 905–907

6 KITAGAWA, T., HATTORI, K., SHUTO, K., YASU, M., KOBAYASHI, M., and HORIGUCHI, M.: 'Amplification in erbium-doped silica-based planar lightwave circuits', *Electron. Lett.*, 1992, **28**, pp. 1818–1819

# Experimental evidence of pseudo-periodical soliton propagation in dispersion-managed link

F. Favre, D. Le Guen and T. Georges

The first experimental evidence of pseudo-periodical soliton propagation in a dispersion-managed link is presented. It is shown that the prechirp is a key element for the control of nonlinearity as predicted by the theory.

*Introduction:* Soliton transmission is widely studied for large capacity transoceanic and terrestrial systems. Since the most common embedded fibre is standard step-index fibre, periodical dispersion compensation is required to upgrade long-distance terrestrial systems beyond 5Gbit/s per channel [1]. In this context, soliton WDM transmission of 16 channels, each modulated at 20Gbit/s, has recently been demonstrated over 1300km of standard fibre with 100km dispersion-compensated spans [2].

The aim of this study is to compare measured and predicted pulse evolution along a dispersion-managed link in the anomalous-dispersion regime using a recirculation loop with 100km dispersion-compensated span of standard fibre, as in [2].

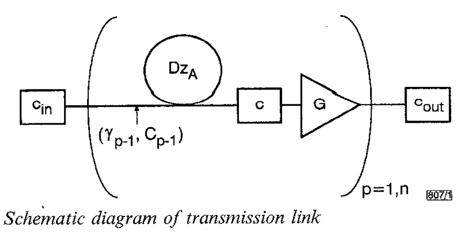


**Fig. 1** *Schematic diagram of transmission link*

*Theoretical background:* The periodic line is shown in Fig. 1. $c_{in}$ is the cumulative dispersion of the element controlling the prechirp at the emitter. The span $z_A$ with dispersion $D$ is followed by a dispersion compensation unit with a cumulative dispersion $c$. We consider in the following the propagation of a single Gaussian pulse in the periodic line assembling $n$ similar steps. The propagation of a pulse $u(z, t) = \sqrt{(a(z))}q(z,t)$ in such a line with dispersion $D(z)$ and energy evolution $a(z)$ can be approximated by the nonlinear Schrödinger equation

$$iq'_z + \frac{1}{2}D(z)q''_{tt} + a(z)|q|^2q = 0 \quad (1)$$

The energy $E = \int_{-\infty}^{+\infty} |q|^2 dt$ is a constant of the motion and the pulse energy along the line is equal to $a(z)E$. In the Gaussian approximation, $q$ can be expressed as

$$q(z,t) = \sqrt{B}\exp\left[-(1+ib)\frac{t^2}{2W^2} + i\phi - i\omega t\right] \quad (2)$$

The pulse width $W$ and the chirp $b$ can be related to two parameters $\gamma$ and $C$ by

$$\gamma W^2 = 1 + \gamma^2 C^2 \quad (3a)$$

$$b = -\gamma C \quad (3b)$$

In the linear regime, $\gamma$ is constant and $C$ corresponds to cumulative dispersion. With nonlinearity, it was shown in [3] that their evolution is governed by the following equations:

$$C'_z = D + \left(C^2 - \frac{1}{\gamma^2}\right)\frac{aE}{W^3\sqrt{2\pi}} \quad (4a)$$

$$\gamma'_z = -2\gamma C\frac{aE}{W^3\sqrt{2\pi}} \quad (4b)$$

Under the specific conditions of propagation studied below, $\gamma$ (which is related to the spectral width) and $C$ change significantly along a span. However, owing to the compensation, they are weakly modified from one span input to the next. The series ($\gamma_p$, $C_p$) of the parameters at the input of each span can be obtained by successive integrations of eqn. 4 over a span. Fig. 2 shows the evolution of ($\gamma_p$, $C_p$) from span to span for different values of prechirp.

Closed trajectories are obtained for initial pulse characteristics different from those of the fixed point (0.65, –1.78) which correspond to steady propagation.

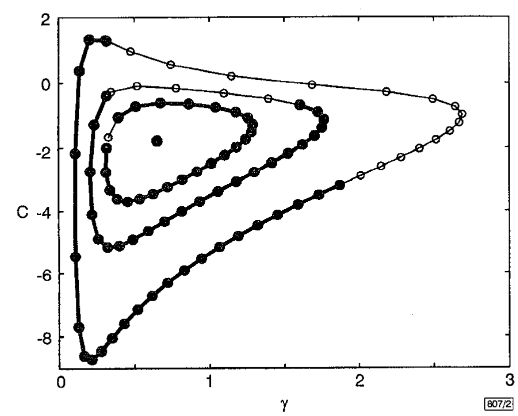


**Fig. 2** *($\gamma_p$, $C_p$) anti-clockwise trajectories calculated from eqn. 4 for experimental conditions (bold lines)*

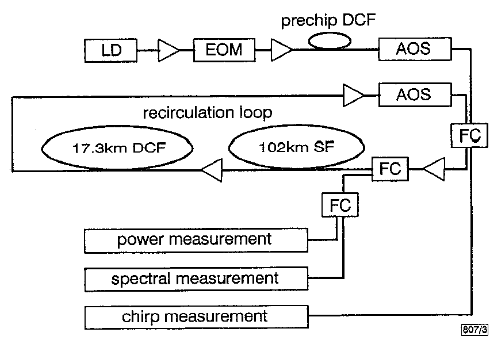


**Fig. 3** *Experimental setup*

*Experimental setup:* The experimental setup is presented in Fig. 3. Nearly Gaussian 30ps pulses are generated at 10GHz for $\lambda$ = 1558nm using a lithium niobate electro-optic modulator (EOM)